Mathematical Modeling of Non-Small Cell Lung Cancer Response to Therapy

Russell Injerd[1], **Emma Turian**[2]

September 22, 2017

Technical Report No. 17-0922

[1] *Northeastern Illinois University, Department of Mathematics, r-injerd@neiu.edu*
[2] *Northeastern Illinois University, Department of Mathematics, m-turian@neiu.edu*

Mathematical Modeling of Non-Small Cell Lung Cancer Response to Therapy

Russell Injerd, Emma Turian

Abstract

Non-small cell lung cancer (NSCLC) represents the largest proportion of lung cancers in the United States. Image guided radiotherapy allows tumor volume dynamics to be measured at certain intervals during treatment. This has improved our ability to study the evolution of tumors such as NSCLC during treatment using time series approach models. The main goal of our research study is to identify the model that best describes the existing radiotherapeutic treatment options: Stereotactic body radiation therapy (SBRT), also known as stereotactic ablative radiotherapy (SABR), and standard therapy (ST). Our mathematical structure builds on the linear quadratic model from the radiation oncological field and therefore, introduces parameters related to tumor's radio-sensitivity. Previous such one and two population ODE models of tumor volume dynamics, treating NSCLC, were designed using exponential and logistic growth functions. These studies indicate that a two population exponential model provided the best balance between fit and mathematical complexity and may serve a functional role in clinical practice. Our study reevaluates previous findings for treating NSCLC using both, the standard and SABR regimens, and tests the suitability of the hyper-Gompertz, hyper-logistic, Richards, Von-Bertalanffy, and a non-linear model derived using fluid mechanics laws by assessing their goodness of fit versus their mathematical complexity. These models are calibrated using data from eleven patients treated using SABR regimen, and four patients treated using standard therapy, extracted from a previous study. Models pertaining both treatment regimens are evaluated using statistical approaches, such as the Akaike Information Criterion. Model comparison indicates that the models fitting patient data perform differently based on the treatment regimen. Our study suggests that for the SABR patients the non-linear model derived from fluid mechanics laws overall outperforms the rest of the studied models, and in the case of the standard treatment the logistic model seems to better represent patient data. Our hope is that our findings will benefit research regarding NSCLC, as well as other cancer field types.

Keywords

Image-guided radiotherapy, dynamic modeling, model selection, non-small cell lung cancer, stereotactic ablative radiotherapy, gross tumor volume.

1 Introduction

Lung cancer, including small and non-small cell, represents the leading cause of cancer death in the U.S., with more people dying of this disease than colon, breast and prostate cancers combined. Among these two different types of lung tumors, non-small cell lung cancer (NSCLC) represents about 85 - 90% of the total number of lung cancers.

There are three known types of NSCLC [17]:

1. **Adenocarcinoma** - a slow growing lung cancer most commonly found on the outer layer of the lung. It is usually found in smokers, but it also represents the most common form of lung cancer in non-smokers.
2. **Squamous cell carcinoma** - in general it develops in the center of the lung. Mostly commonly found in smokers.
3. **Large cell carcinoma** - can occur anywhere in the lung and it usually develops quickly.

It is estimated that in 2017 the number of new cases of lung cancer will reach 222,500 with 155,870 deaths [8]. The non-small cell lung cancer (NSCLC) accounts for 80-85% of all lung cancers [23]. NSCLC includes different subtypes, which originate from different types of lung cells. The reason why these are grouped together as NSCLC is because of their similar treatment type and prognosis. The most prevalent subtypes are as follow: Adenocarcinoma, squamous cell carcinoma and large cell carcinoma, and represent 40%, 25-30%, and 10-15%, respectively of all lung cancers. The number of new cases of lung & bronchus in U.S. for 2017 is expected to reach 116,990 cases for men and 105,510 for women, and the number of deaths is expected to reach 84,500 for men and 71,280 for women. The largest recorded geographic disparity in the U.S. is for lung cancer and reflects the national distribution of poverty and access to care. In the U.S., the highest rate of deaths by lung & bronchus cases is among the non-hispanic black population. It is a well known fact that a major risk factor of lung cancer is the use of tobacco, which in 2010 accounted for .7 million men and .2 million women deaths from the low and middle income categories, versus .4 million men and .2 million women deaths from the high income category [18]. Therefore, a vast proportion of cancer deaths are caused by the use of tobacco, mainly among men, specifically originating from the low and middle income category. Data from the Illinois Department of Public Health reveals that low-income Chicago communities, which are largely African-American or Latino, have

cancer rates up to double the national average. In Illinois, the estimated number of new cases of lung & bronchus cancer is 8,600 with 6,470 estimated deaths in 2017 [4]. In Illinois, the number of male lung & bronchus cases exceed that of female cases (the incidence rates are 81 male versus 58.5 female per 100,000 during 2009-2013) [4].

Despite the successes obtained by the latest advancement in detection and treatment and the reduction in the use of tobacco, the fight against cancer requires advancements in basic research to improve both detection and treatment.

The main goal of our research study is to identify the best model that fits the following two treatment options: Stereotactic body radiation therapy (SBRT), also known as stereotactic ablative radiotherapy (SABR), and standard therapy (ST) for NSCLC. Both regimen options use image-guided radiation therapy as a tool for improving the precision and accuracy of treatment delivery.

SABR represents a choice of treatment that gives a large dose of radiation concentrated at the tumor, while the neighboring organs receive limited amounts of that radiation. This treatment option represents a recent implementation in the field of radiation oncology, promises high rates of local control for NSCLC, and represents a good alternative for non-surgical tumors. In our study, we use linear and non-linear simulations for empirical, as well as theoretical models. The goal of our study is to estimate parameter values, which lead to predictive conclusions regarding tumor dynamics under therapy, and the validity of our models. Behavior of such quantities and their evolution across models and patient data may help assist the radiation oncologists in the development of dosing recommendations.

Fitting results from our numerical simulations suggest that not only that models apply differently to patient data, but also, they differ from one treatment regimen to the other. For the SABR patients the non-linear model derived from fluid mechanics laws overall outperforms the rest of the studied models, and for the standard treatment the logistic model seems to better represent patient data. Results also suggest that using a heterogeneous two population model, the evolution under therapy of the two populations, live and dead, can be described as "simple" and "crossed". These behaviors differ from model to model with an exponential incline more towards the "simple" case. A discussion regarding parameter findings can be found inside the Conclusions Sections.

Our mathematical model distinguishes from the majority of existing approaches in that it makes use of the linear quadratic model used in the radiation oncological field and therefore, includes parameters related to tumor's radio-sensitivity. Our hope is that using predictions related to these two treatment regimens, oncologists can better choose between the most effective and less toxic alternative for their lung cancer patients.

The outline of our paper is as follows. In Section 2, we introduce the

methodology, the ODE models, results from numerical simulations, and statistical analysis. In Section 3, we draw conclusions related to each treatment regimen. In Section 4, we discuss shortcomings related to using our models and future work.

2 Methods

Our study investigates the tumor dynamics using patient data representing gross tumor volume (GTV), for NSCLC patients, treated using the SABR and standard regimens. Our model assumes that tumor cell population is heterogeneous, and therefore divided into live and dead cells. Patient data originating from two datasets [21] were used for this study. Individual patient data was fitted to our model and parameter values were used to create inferences about the appropriateness of the models used in this study.

The linear-quadratic equation will be used to model the effects of radiotherapy. After each fractionated dose a proportion of the cells will die and the remainder of the cells survive treatment.

The surviving fraction, S [Appendix C], can be written

$$S = \exp(-\alpha d - \beta d^2), \tag{1}$$

where S represents the surviving fraction, d is the dose per fraction, and α and β are the linear and quadratic coefficients, representing tumor radiosensitivity. To limit the infinite combinations of α and β the ratio is fixed to 10 Gy^{-1}, thereby requiring estimation of α only.

2.1 ODE model

Our study explicitly investigates the tumor dynamics using patient data representing gross tumor volume (GTV), for NSCLC patients, treated using the SABR and standard regimens. Our model assumes that tumor cell population is heterogeneous, and therefore divided into live and dead cells. Our mathematical model includes a "point-to-point" approach used to fit GTV data in order to find parameter values. Using the linear-quadratic described by Eq. 1, the "point-to-point" method is described by the following scheme [20]

$$\begin{cases} V_l(t + \Delta t) = V_l(t)S, \\ V_d(t + \Delta t) = V_d(t) + V_l(t)[1 - S], \end{cases} \tag{2}$$

with (Δt) representing an infinitesimal amount of time after the fractionated dose is delivered, and the scheme

$$\begin{cases} \frac{dV_l}{dt} = f(V_l), \\ \frac{dV_d}{dt} = -cV_d, \\ V = V_l + V_d, \end{cases} \tag{3}$$

where $f(V_l)$ is the growth term, V_l is the volume of living tumor cells, V_d is the volume of dead cells, and c is the clearance rate.

Figure 1 summarizes the method used to model GTV at the time each fractionated dose is delivered.

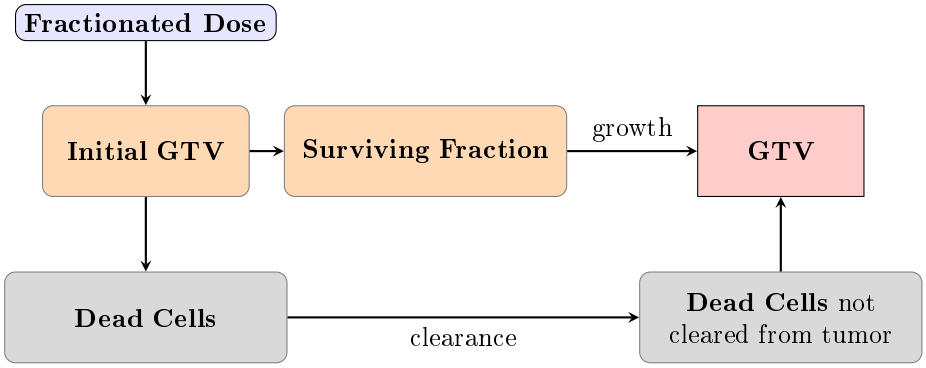

Figure 1: Two population tumor growth model.

To accomplish this, several ODE models for tumor growth were considered. Tariq et. al. [20] studied a two population model with the growth terms described by exponential and logistic functions. Exponential growth assumes that all vital nutrients are available in abundance and places no constraints on growth. This assumption is reasonable for small tumors like stage 1 NSCLC with tumor diameter less than 5 cm [21]. We expand these approaches and consider growths described by functions with empirical grounds as well as non-linear functions derived from theoretical fluid mechanics laws.

The ODE growth models for the live cell population representing Eq. (3a), can be described as follow:

- Exponential
$$\frac{dV_l}{dt} = kV_l, \tag{4}$$
- Hyper-logistic
$$\frac{dV_l}{dt} = kV_l^{\eta}\left(1 - \frac{V_l}{M}\right)^{\zeta}, \tag{5}$$
with $\eta = 1$ and $\zeta = 1$. Parameter M represents the carrying capacity.
- Hyper-Gompertz
$$\frac{dV_l}{dt} = kV_l\left(\ln\frac{M}{V_l}\right)^{\gamma}, \tag{6}$$
with $\gamma = 1$.

- Richards

$$\frac{dV_l}{dt} = kV_l\left(1 - \left(\frac{V_l}{M}\right)^{\gamma}\right). \tag{7}$$

- Von-Bertalanffy

$$\frac{dV_l}{dt} = kV_l^{\frac{2}{3}}\left(1 - \left(\frac{V_l}{M}\right)^{\frac{1}{3}}\right). \tag{8}$$

- A dimensional radial growth model based on Darcy's Law includes diffusion length and vasculature parameters [10]. The radial growth model can be written

$$\frac{dV_l}{dt} = 3^{2/3}(4\pi)^{1/3}kL(1-B)V_l^{2/3} + kBV_l, \tag{9}$$

where $L = 0.007$ is the diffusion length and $B = 0.54$ is the vasculature [11].

Model	Abbreviation	Parameters	Growth Term Equation #
Exponential	EXP	α, k, c	4
Logistic	LOG	α, k, M, c	5
Gompertz	GOM	α, k, M, c	6
Richards	RIC	α, k, M, c, γ	7
Von Bertalanffy	VB	α, k, M, c	8
Radial	3D	α, k, c	9

Table 1: Summary of models.

2.2 Numerical implementation

Numerical implementation for the models described in this section include a combination of random search procedures, using pseudo-random seeds, and interior point methods. Linear and non-linear solvers were constructed to allow for numerical results of the "point-to-point" scheme described by Eq. (2). In some circumstances, when the number of data points were small and analytical solutions were computationally permissive, models were plotted as continuous piecewise functions. This allowed for further statistical analysis to be conducted including confidence bands. In other cases, solution recursion and numerical solving methods were too computationally expensive to permit plotting continuous solutions and the "point-to-point" scheme was used to study model behavior. The varying methods of plotting did not impact parameter fitting or model comparison statistics.

2.3 Uncertainty analysis and parameter estimation

Models are calibrated to each patient by estimating the model parameters listed in table 1 using the maximum likelihood estimation (MLE), where the sum-of-squares error (SSE) [2]

$$SSE = \sum_{t=1}^{T} \left(V(t, \mathbf{p}) - v_t\right)^2, \tag{10}$$

where V is the measured GTV right before the t^{th} fraction, $\mathbf{p}$ is the parameter vector including the error σ, T is the total number of fractions for an individual patient, and v_t is the corresponding modeled GTV. Constrained optimization is conducted for model parameters using a combination of random search, using pseudo random seeds, and interior point methods. Constraints are chosen to allow freedom for models to fit individual patients' response to radiotherapy.

Parameter constraints for each dataset are shown in tables 2 and 3.

Parameter	Description	Units	Constraints
k	proliferation rate	d^{-1}	[.001-.999]
α	radio-sensitivity parameter	Gy^{-1}	[.001-.999]
M	carrying capacity	cc	[$V_{(0)}$ - 100]
c	clearance rate for dead cells	d^{-1}	[.001-.999]
γ	shape exponent	-	[.001-10]

Table 2: SABR model parameters.

Parameter	Description	Units	Constraints
k	proliferation rate	d^{-1}	[.001-.999]
α	radio-sensitivity parameter	Gy^{-1}	[.001-.999]
M	carrying capacity	cc	[$N_{(0)}$ - 1000]
c	clearance rate for dead cells	d^{-1}	[.001-.999]
γ	shape exponent	-	[.001-10]

Table 3: Standard therapy model parameters.

To limit the infinite combinations of the radio-sensitivity parameters α and β, the ratio is fixed to 10 Gy^{-1}, thereby requiring estimation of α only. Since the number of parameters for some of the considered models exceeds existing data points, some were kept fixed (i.e. the diffusion length, $L = 0.007$, and the vascularization parameter, $B = 0.54$ [11]). Pearson correlation analysis is also performed to determine statistically significant dependencies between estimated parameters. Some of the parameters show high correlation as shown in table 4 for the models under consideration. Correlation values

close to 1 indicate that it may not be possible to estimate respective parameters separately. Table 4 suggests that such high correlation exists between parameters α and k, suggesting a positive high dependence for the Gompertz and logistic models for the standard regimen and 3D model for the SABR regimen. Another such high dependence exists between the carrying capacity, M, and clearing rate, c, for the same Gompertz and logistic models used for standard regimen.

		α	M	c
3D	α	-	-	-
	k	-	-	-
EXP	α	-	-	-
	k	-	-	-
GOM	α	-	-	-
	k	0.9957	-	-
	M	-	-	0.98
LOG	α	-	-	-
	k	-	-	-
	M	-	-	0.9848

		α	M	c
3D	α	-	-	-
	k	0.96	-	-
EXP	α	-	-	-
	k	-	-	-
GOM	α	-	-	-
	k	0.742	-	0.659
	M	-	-	-
LOG	α	-	-	-
	k	-	-	-
	M	-	-	-

Table 4: Statistically significant (p-value$<$0.05) parameter correlation statistic. Left: standard therapy regimen. Right: SABR regimen.

To assess goodness of fit the % root mean squared error ($\%RMSE$) is used by first finding the root mean squared error given by

$$RMSE = \sqrt{SSE/T}, \tag{11}$$

then dividing by the mean of measured patient GTV $\bar{V}$, written as

$$\%RMSE = RMSE/(\bar{V}) * 100\%. \tag{12}$$

Given a group of candidate models, an information-theoretic approach for selection is used. A model with more parameters tends to fit data better than a model with fewer parameters. However, there is a tradeoff when increasing the number of free parameters between decreasing bias and increasing variance [3]. Therefore, model selection using $\%RMSE$ alone will likely result in over-fitting and high uncertainty.

2.4 Model comparison for the standard treatment and SABR regimens

To achieve a balance between model fit and model complexity and select a parsimonious model, Akaike's Information Criterion AIC is used to compare models for each patient. AIC can be written as

$$AIC = T(\ln(2\pi) + \ln(SSE/T) + 1) + 2p, \tag{13}$$

where p is the number of free parameters including the variance. AIC is a heuristic estimator of the more rigorous Kullback-Liebler distance that measures the discrepancy between distributions [3]. AIC rewards model fit while penalizing free parameters to rank a set of candidate models. When dealing with small samples, as is often the case in oncological modeling, AIC may lead to over-fitting. When possible, a small sample corrected method $AICc$ [12] is used given by

$$AICc = AIC + \frac{2p(p+1)}{T-p-1}. \tag{14}$$

Though not ideal, AIC is used for the 5 sample SABR data, as calculating $AICc$ results in comparing infinite values. The AIC difference (Δ_i) for model i is calculated using

$$\Delta_i = AIC_i - AIC_{min}, \tag{15}$$

or

$$\Delta_i = AICc_i - AICc_{min}, \tag{16}$$

when $AICc$ is calculable. As a general rule, candidate models with $\Delta_i < 2$ have substantial support, $4 < \Delta_i < 7$ have considerably less support, and $\Delta_i > 10$ might be omitted from future consideration [3]. Δ_i is also useful for calculating Akaike Weights (w_i) given by

$$w_i = \frac{\exp(-0.5\Delta_i)}{\sum_{r=1}^{R} \exp(-0.5\Delta_r)}, \tag{17}$$

which gives the relative likelihood for each of the candidate models. The w_i can be interpreted as the probability that model i is the best model, given the data and set of candidate models (Δ_r) [3].

Patient	Model	p	$\%RMSE$	AIC	$AICc$	Δ_i	w_i
1	3D	4	7.57	3.31	**16.65**	0	0.50
	EXP	4	7.58	3.33	16.66	0.01	0.498
	LOG	5	7.55	5.28	35.28	18.63	0.00005
	GOM	5	8.69	7.52	37.52	20.87	0.00001
2	3D	4	4.93	-11.55	**1.78**	0	0.52
	EXP	4	5.12	-11.33	2.00	0.22	0.46
	GOM	5	2.95	-20.57	9.43	7.65	0.01
	LOG	5	2.54	-20.16	9.84	8.06	0.009
3	EXP	4	1.23	**7.15**	∞	0	0.45
	3D	4	1.25	7.36	∞	.21	0.40
	LOG	5	1.27	9.46	∞	2.32	0.14
	GOM	5	2.37	15.7	∞	8.6	0.006
4	EXP	4	2.50	**5.12**	∞	0	0.36
	3D	4	2.50	5.12	∞	0.001	0.36
	LOG	5	2.49	7.08	∞	1.96	0.14
	GOM	5	2.50	7.12	∞	2.01	0.13
5	3D	4	2.09	**15.2**	∞	0	0.38
	EXP	4	2.09	15.2	∞	0.0006	0.37
	LOG	5	2.09	17.25	∞	2.0	0.14
	GOM	5	2.11	17.3	∞	2.06	0.13
6	3D	4	9.83	**18.7**	∞	0	0.36
	EXP	4	9.84	18.7	∞	0.002	0.36
	GOM	5	9.61	20.5	∞	1.77	0.15
	LOG	5	9.83	20.75	∞	2.0	0.13
7	EXP	4	2.86	**5.14**	∞	0	0.37
	3D	4	2.86	5.15	∞	0.006	0.37
	LOG	5	2.86	7.15	∞	2.01	0.14
	GOM	5	2.95	7.47	∞	2.33	0.12
8	EXP	4	0.82	**-1.14**	∞	0	0.65
	3D	4	0.75	0.21	∞	1.35	0.33
	LOG	5	1.45	8.86	∞	8.94	0.007
	GOM	5	1.30	7.8	∞	10.0	0.004
9	GOM	5	0.79	**-5.99**	∞	0	0.999
	EXP	4	4.48	9.35	∞	15.34	0.0005
	LOG	5	4.48	11.4	∞	17.34	0.0002
	3D	4	6.01	12.3	∞	18.28	0.0001
10	GOM	5	0.14	**-10.21**	∞	0	0.67
	EXP	4	0.22	-7.52	∞	2.68	0.18
	LOG	5	0.22	-5.90	∞	4.30	0.08
	3D	4	0.27	-5.68	∞	4.52	0.07
11	EXP	4	0.83	**-1.14**	∞	0	0.36
	3D	4	0.83	-1.14	∞	.0001	0.36
	LOG	5	0.39	0.12	∞	1.26	0.19
	GOM	5	0.88	1.5	∞	2.64	0.01

Table 5: SABR model statistics.

Patient	Model	p	$\%RMSE$	AIC	$AICc$	Δ_i	w_i
2	LOG	5	2.65	275	**277**	0	0.999
	EXP	4	3.50	290.93	292	15.04	0.0005
	3D	4	3.69	294.31	296	18.42	0.0001
	GOM	5	3.93	300.27	303	25.21	$3.4 * 10^{-6}$
3	EXP	4	10.86	232.51	**234**	0	0.36
	3D	4	10.94	232.95	235	0.45	0.28
	LOG	5	10.56	233	235	1.26	0.19
	GOM	5	10.60	233.08	236	1.48	0.17
4	LOG	5	5.96	266	**268**	0	0.53
	GOM	5	6.05	266.91	269	0.97	0.33
	3D	4	6.47	269.34	271	2.61	0.14
	EXP	4	7.49	278.99	280	12.26	0.001
9	EXP	4	2.37	107.85	**110**	0	0.36
	3D	4	2.37	107.84	110	0.44	0.28
	LOG	5	2.30	108.19	111	1.26	0.19
	GOM	5	2.37	110	113	1.48	0.17

Table 6: Standard therapy model statistics.

2.5 Radio-sensitivity parameter α analysis

The two radio-sensitivity parameters α (Gy^{-1}) and β (Gy^{-2}) are constants, one representing the linear and the other the quadratic component [Appendix C], characteristic to a certain tumor or tissue. In order to limit the number of varying parameters we consider that $\frac{\alpha}{\beta} = 10$, and allow fitting for α parameter only.

Tables with values for parameter α from all the numerical simulations are listed in table 7 for the SABR regimen patients, and in table 8 the standard therapy patients included in this study. Table 7 suggests that the logistic model provides on average the highest α value, while the $3D$, the lowest. Since values for this parameter are believed to be around 0.3 [15], we conclude that for this reason only, the logistic model outperforms the rest of the studied models for the SABR case. The standard therapy results, shown in table 8, suggests that the Logistic and Gompertz models indicate larger values for parameter α. Therefore, if 0.3 is believed to best approximate this parameter, then the standard regimen seems to be better represented by the Gompertz and Logistic models.

The high correlation between α and k shown in table 4 means that a larger mitosis rate, k, means a higher α value. While high parameter correlation is an unwanted feature, from a radio-biological perspective this correlation has an expected significance.

Patient no.	3D	EXP	GOM	LOG
1	0.084	0.085	0.211	0.083
2	0.066	0.063	0.161	0.145
3	0.113	0.119	0.044	0.120
4	0.054	0.053	0.13	0.064
5	0.005	0.005	0.047	0.005
6	0.015	0.015	0.046	0.043
7	0.020	0.020	0.026	0.020
8	0.007	0.004	0.14	0.50
9	0.004	0.948	0.109	0.923
10	0.007	0.027	0.018	0.026
11	0.004	0.004	0.152	0.011
Average	0.0345	0.1221	0.0985	0.176

Table 7: Parameter α for the SABR regimen.

Patient no.	3D	EXP	GOM	LOG
2	0.020	0.021	0.021	0.015
3	0.051	0.052	0.245	0.130
4	0.014	0.027	0.136	0.058
9	0.999	0.999	0.770	0.999
Average	0.099	0.100	0.124	0.109

Table 8: Parameter α values for the standard regimen.

2.6 Numerical results

Subsections below include simulation results for the growth models considered in this study, and their appropriate confidence bands where possible. SABR patient data includes the dynamics for their respective GTVs for two types of dose fractionation: One arriving from the simulation of two patient data with eight data points (patients 1 and 2), and another from the simulation of nine patient data with five data points (patients 3 through 11). The former category of patients was treated with 7.5 Gy per fraction and the latter with 11 Gy per fraction. Plots representing patient GTV data and numerical simulation results allow for significant differences in prediction behavior. These plots suggest the following. While Figs. 2 and 3 for SABR patients 1 and 2 suggest a fairly constant change in tumor dynamics, patients represented by a reduced number of data points, exhibit a non-constant amount of uncertainty. This could be explained because the larger prescribed dose received by the latter category of patients may induce inflammation over different time intervals. Wider confidence bands for the 5-data points versus 8-data points SABR patients might suggest increased inflammation due to a higher administered dose. Numerical runs for the standard regimen and

for the 3D model do not include confidence bands, because of the methodology used for obtaining the results. From the exponential, Gompertz, and logistic models, the last two seem to provide wider and non-uniform confidence bands. The mean confidence intervals (not shown here) have all data points included in the widest band interval, suggesting that our models might represent a good fit for the type of patient data included in this study.

Our model suggests that the two subpopulations of tumor cells, live and dead, have different behavior which varies from model to model, as well as from patient to patient. The two types of behavior can be regarded as "simple" (i.e. Figs. 6, 7, 8, 9, 10, 20, 22), and "crossed" (i.e. Figs. 11, 18, 19, 21, 23). These two differences are reflected in the clearance coefficient, c. Large c values (i.e. > 0.5 indicates a "simple" behavior, while a smaller c indicates a "crossed" pattern. More research needs to be performed to establish a bifurcation parameter value for these cases. Among the models included in this study the exponential model seems to include the highest clearance rates.

2.6.1 Exponential Model

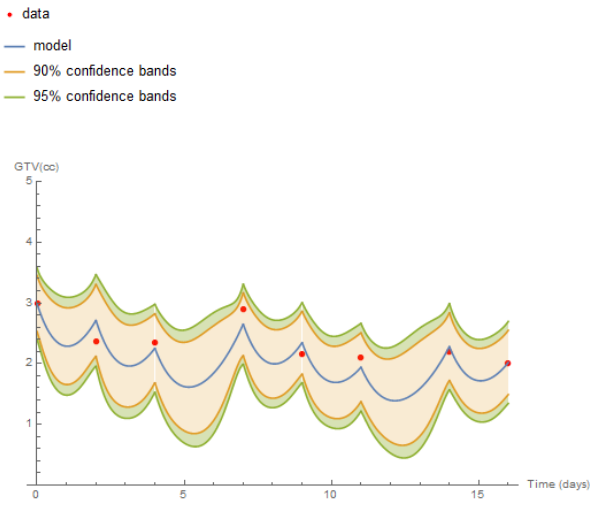

Figure 2: SABR Patient 1 EXP: $\alpha = 0.085$, $k = 0.456$, $c = 0.999$.

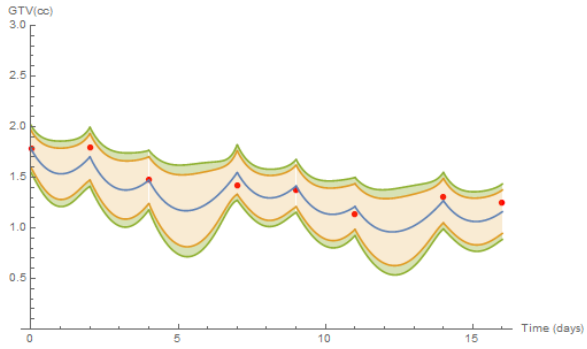

Figure 3: SABR Patient 2 EXP: $\alpha = 0.063$, $k = 0.328$, $c = 0.784$.

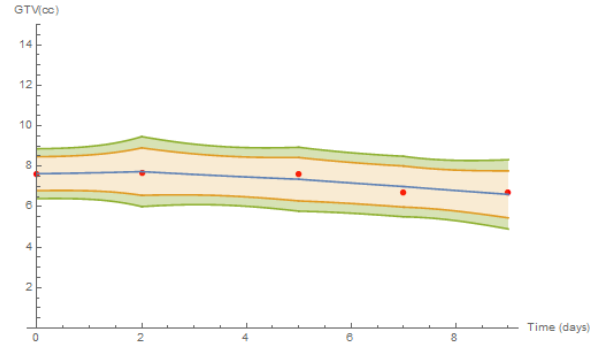

Figure 4: SABR Patient 4 EXP: $\alpha = 0.053$, $k = 0.087$, $c = 0.030$.

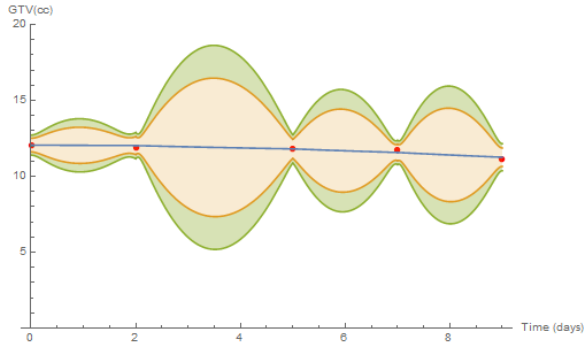

Figure 5: SABR Patient 8 EXP: $\alpha = 0.004$, $k = 0.005$, $c = 0.067$.

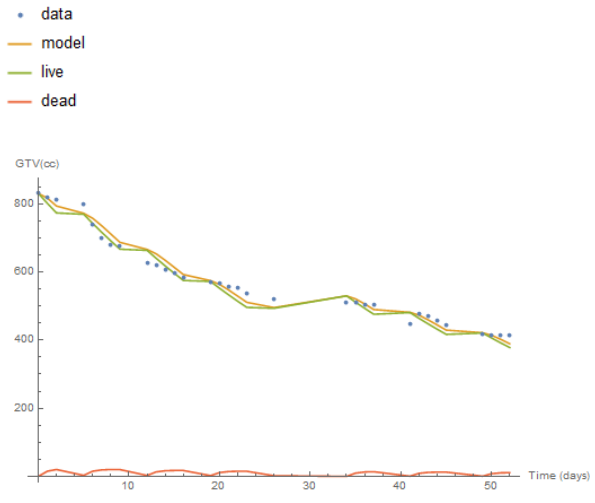

Figure 6: ST Patient 2 EXP: $\alpha = 0.021$, $k = 0.015$, $c = 0.999$.

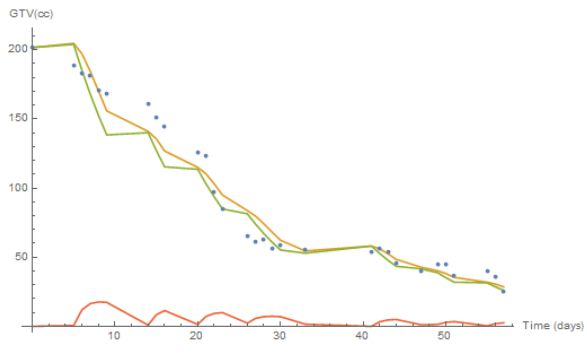

Figure 7: ST Patient 3 EXP: $\alpha = 0.052$, $k = 0.027$, $c = 0.713$.

2.6.2 3D Model

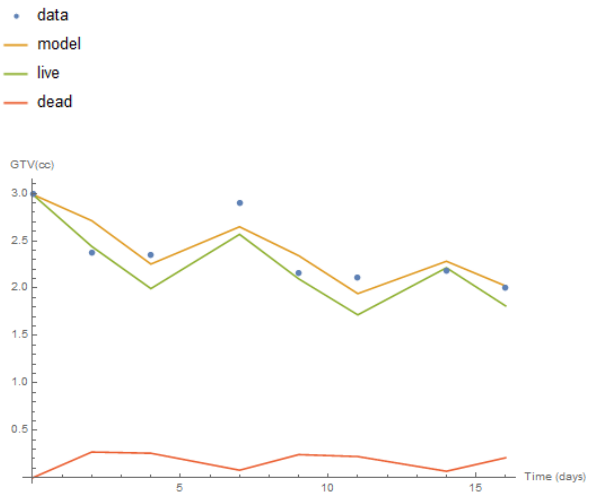

Figure 8: SABR Patient 1 3D: $\alpha = 0.084$, $k = 0.818$, $c = 0.999$.

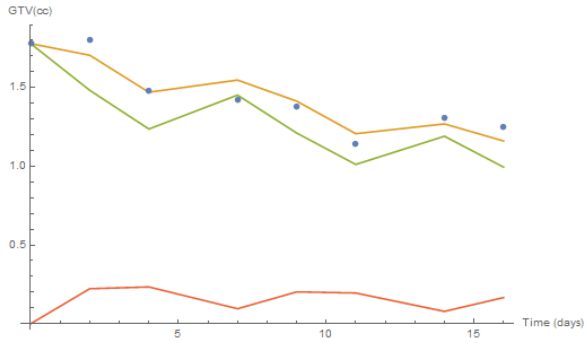

Figure 9: SABR Patient 2 3D: $\alpha = 0.066$, $k = 0.615$, $c = 0.766$.

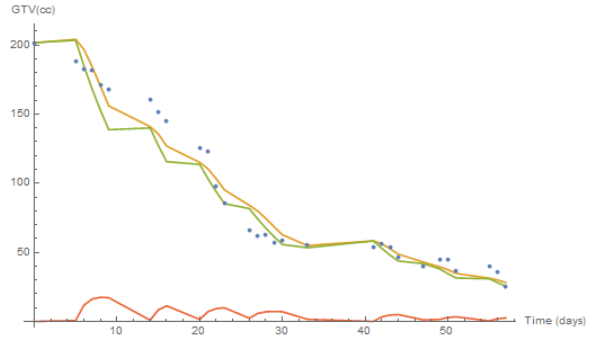

Figure 10: ST Patient 3 3D: $\alpha = 0.051$, $k = 0.048$, $c = 0.711$.

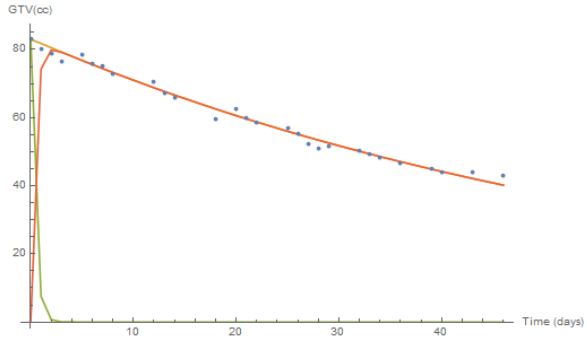

Figure 11: ST Patient 9 3D: $\alpha = 0.999$, $k = 0.001$, $c = 0.016$.

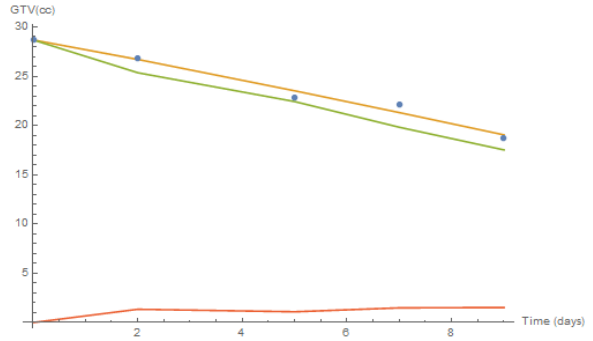

Figure 12: SABR Patient 5 3D: $\alpha = 0.005$, $k = 0.001$, $c = 0.457$.

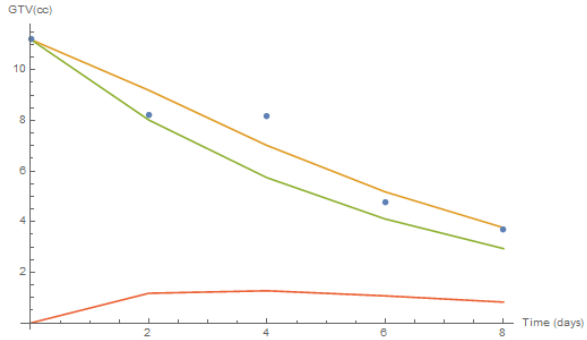

Figure 13: SABR Patient 6 3D: $\alpha = 0.015$, $k = 0.001$, $c = 0.500$.

2.6.3 Gompertz Model

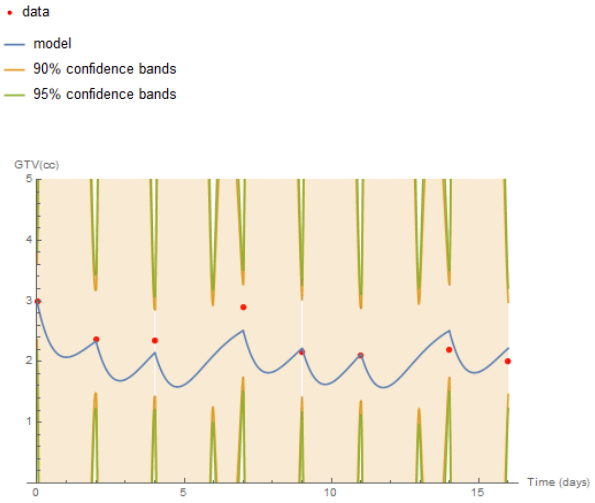

Figure 14: SABR Patient 1 GOM: $\alpha = 0.211$, $k = 0.999$, $M = 45.056$, $c = 0.999$.

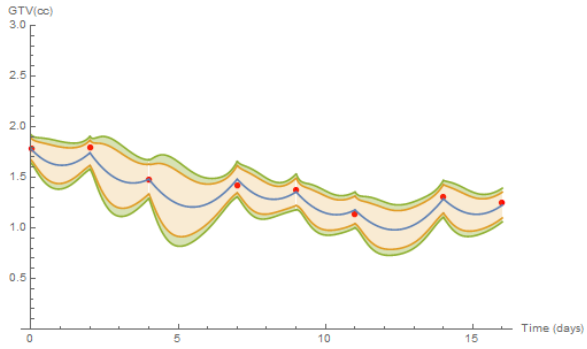

Figure 15: SABR Patient 2 GOM: $\alpha = 0.161$, $k = 0.267$, $M = 61.237$, $c = 0.330$.

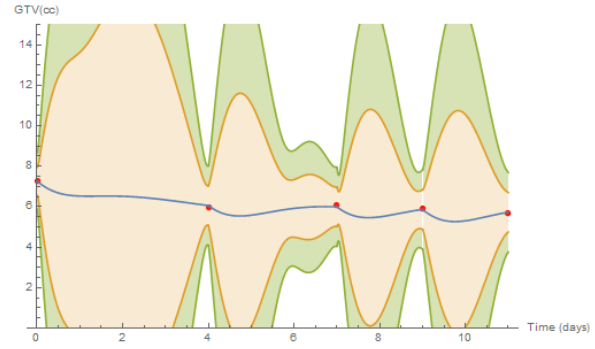

Figure 16: SABR Patient 9 GOM: $\alpha = 0.109$, $k = 0.999$, $M = 65.356$, $c = 0.466$.

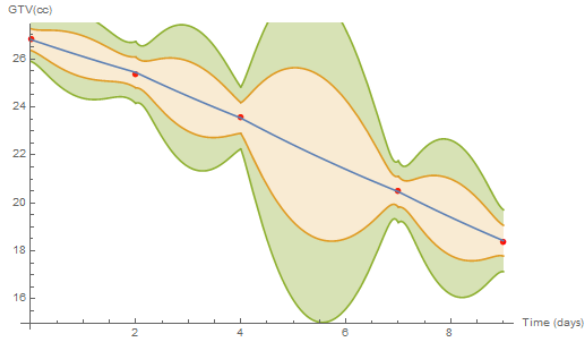

Figure 17: SABR Patient 10 GOM: $\alpha = 0.018$, $k = 0.019$, $M = 27.893$, $c = 0.082$.

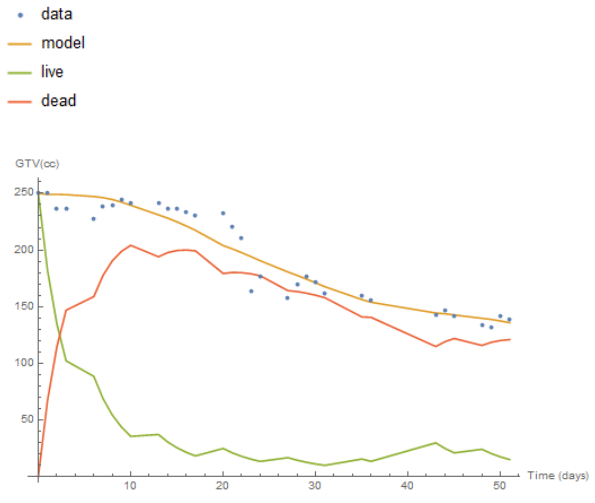

Figure 18: ST Patient 4 GOM: $\alpha = 0.136$, $k = 0.066$, $M = 282.091$, $c = 0.033$.

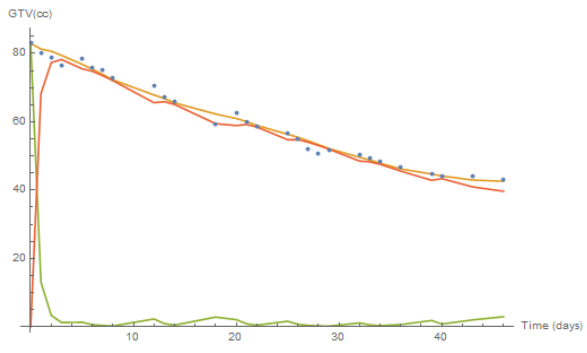

Figure 19: ST Patient 9 GOM: $\alpha = 0.770$, $k = 0.304$, $M = 83.190$, $c = 0.024$.

2.6.4 Logistic Model

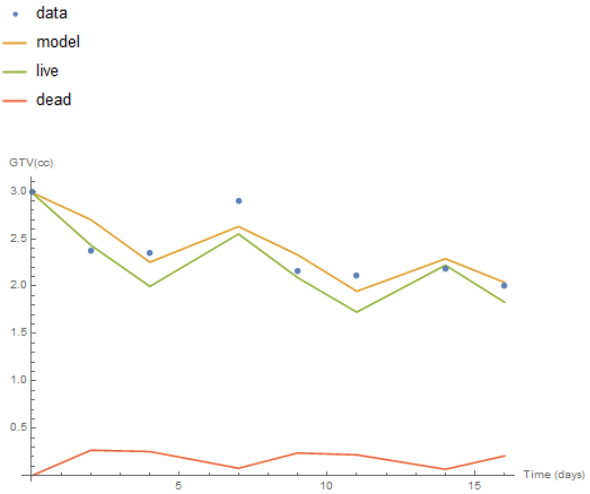

Figure 20: SABR Patient 1 LOG: $\alpha = 0.083$, $k = 0.467$, $M = 31.19$, $c = 0.999$.

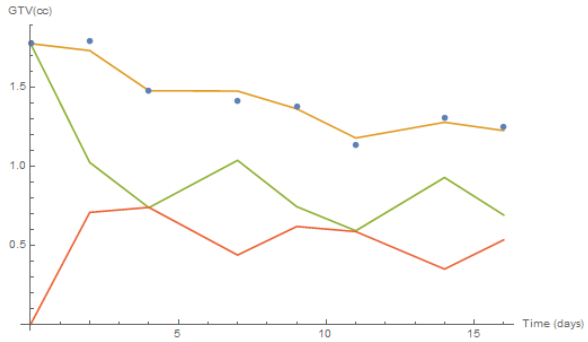

Figure 21: SABR Patient 2 LOG: $\alpha = 0.145$, $k = 0.999$, $M = 1.87$, $c = 0.379$.

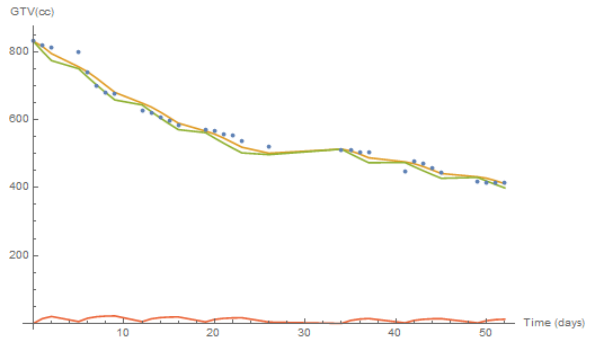

Figure 22: ST Patient 2 LOG: $\alpha = 0.015$, $k = 0.022$, $M = 830.79$, $c = 0.739$.

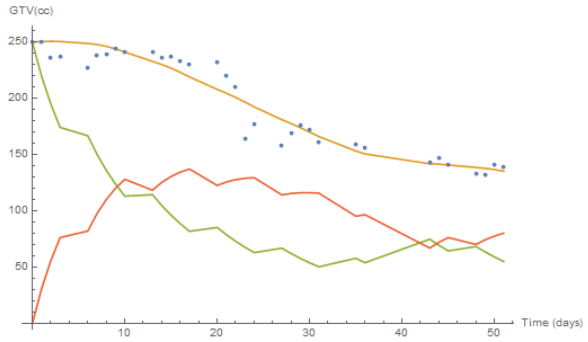

Figure 23: ST Patient 4 LOG: $\alpha = 0.058$, $k = 0.088$, $M = 250$, $c = 0.062$.

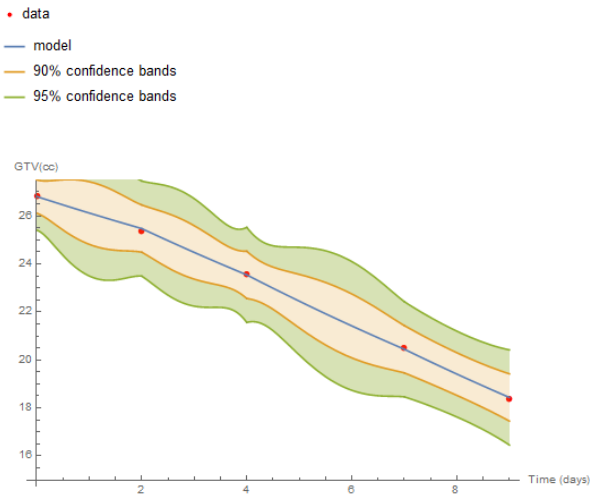

Figure 24: SABR Patient 10 LOG: $\alpha = 0.026$, $k = 0.001$, $M = 26.81$, $c = 0.059$.

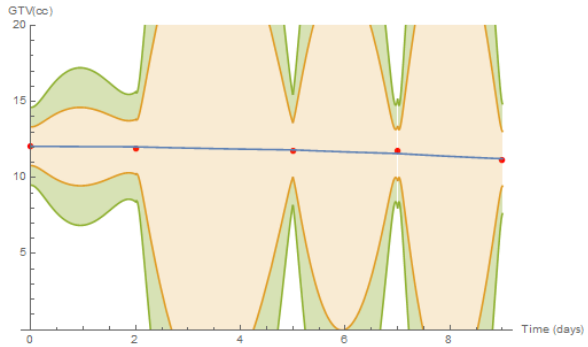

Figure 25: SABR Patient 11 LOG: $\alpha = 0.01$, $k = 0.077$, $M = 12.06$, $c = 0.068$.

3 Conclusions

Results for SABR and standard therapy data sets include model fit and selection statistics as well as patient α values. Fit and selection statistics were calculated for EXP, 3D, GOM, and LOG models. Because of the inclusion of γ, it was expected that the RIC models would match or outperform LOG models when compared using $\%RMSE$. Generally, RIC models underperformed compared to LOG models due to rounding errors in the numerical solving methods. Parameter estimation for the RIC model was also computationally expensive. For these reasons it was determined that the study would not benefit from further evaluation of the RIC models. Von-Bertalanffy growth model is a particular case of the general logistic function, we excluded this model from our list since outcomes did not significantly differ from the logistic model. Model comparison using existing criterion include AIC and AICc, since BIC require large sample sizes for convergences, which we were not able to acquire for our study.

Fitting results suggest that model parameters vary from patient to patient and from model to model. Parameters α and the mitosis rate, k show high correlation for most of the models under consideration. The clearance rate, c, divides the two cell population evolution into two distinct patterns: "simple" and "crossed", which vary between patients and models.

3.1 SABR

Model fit and selection results for SABR patients can be found in table 5. Results indicate strong support for both EXP and 3D models, which combined, are ranked as the best fit for 9 of the 11 SABR patients. For EXP and 3D models, only 1 patient has $\Delta_i > 7$, indicating that these models merit consideration in most SABR patients relative to LOG and GOM models. While EXP and 3D models performed similarly, α values for EXP models were less consistent. 3D models may offer better reliability when using clinical data. GOM models were the worst performing models for SABR data with $\Delta_i > 7$ in 4 of the patients. GOM models also have significantly correlated α, k, and c values (table 4), indicating that the parameter values are not fully identifiable. Confidence bands for GOM and LOG models produced very large intervals for GTV, for many patients the lower bands were below 0. The inclusion of a M parameter may not be worth including in modeling GTV for SABR patients as it adds considerable uncertainty, and it is unlikely that small stage 1 tumors are close enough to a carrying capacity to significantly differ from exponential growth within the 2-3 week treatment window. Our analysis regarding the residuals is shown in [Appendix: A]. Large values resulting from the Kolmogorov-Smirnov test indicate residual normality for all SABR patients and all models.

3.2 Standard therapy

Model fit and selection results for standard therapy patients can be found in table 6. For this treatment regimen, results for α indicate strong support for the

Gompertz model. However, Gompertz models fit poorly when compared to LOG models. Poor α estimation results could be the result of fixing the α/β ratio to $10Gy$, which may not represent this clinical cohort. LOG $\Delta_i < 2$ for each patient and w_i values were above 0.5 for 2 of 4 patients. In contrast to SABR, the inclusion of a M parameter suggests improved modeling results. This may be because initial tumor volumes of patients receiving standard therapy are larger and more likely to be near a carrying capacity. This would cause the shape of LOG models to significantly differ from exponential growth. The data which the LOG model explained the poorest had a relatively small initial tumor volume. This suggests that the LOG models may better fit larger tumor dynamics. Our analysis regarding the residuals is shown in [Appendix: B]. Large values (with the exception of one p-value) resulting from the Kolmogorov-Smirnov and Cramer-von Mises tests indicate residual normality for all standard patients under consideration and all models.

4 Future Work

One of the shortcomings of our approach included fixing the α/β ratio to 10. Therefore, we would like that our future work includes estimations of such fraction. On the other hand, we would like to focus on the meaning of our parameter values and consider the possibility of modifying existing models, based on statistical findings related to individual parameters.

We would also like to next consider patient population inference and Bayesian statistics.

5 Acknowledgments

The authors of this project gratefully acknowledge the support of the Chicago Cancer Health Equity Collaborative Grant funding for the Summer Faculty-Student Cancer-Related Research for 2017.

A SABR Residual Normality Test

Patient no.	3D	EXP	GOM	LOG
1	0.976	0.947	0.594	0.997
2	0.927	0.927	0.462	0.509
3	0.963	0.964	0.61	0.917
4	0.984	0.984	0.923	0.968
5	0.821	0.824	0.816	0.992
6	0.424	0.424	0.346	0.325
7	0.572	0.571	0.668	0.694
8	0.509	0.532	0.387	0.572
9	0.652	0.118	0.53	0.118
10	0.683	0.951	0.466	0.978
11	0.532	0.532	0.517	0.427

Table 9: Kolmogorov-Smirnov p-values.

B Standard Therapy Residual Normality Test Statistic

Patient no.	Test_{3D}	3D	Test_{EXP}	EXP	Test_{GOM}	GOM	Test_{LOG}	LOG
2	CVM	0.429	CVM	0.291	CVM	0.924	CVM	0.779
3	CVM	0.721	CVM	0.657	CVM	0.302	CVM	0.714
4	CVM	0.396	CVM	0.838	CVM	0.295	CVM	0.07
9	KS	0.201	KS	0.197	KS	0.07	KS	0.02

Table 10: Cramer-von Mises (CVM) or Kolmogorov-Smirnov (KS) p-values.

C Surviving Fraction

Given a total dose, D, the cell surviving fraction S after radiation can be expressed mathematically [16]

$$S = e^{-\alpha D} e^{-\beta D^2}, \tag{18}$$

which includes the *linear* and *quadratic* components. Here α and β are tumor characteristics measured in Gy^{-1} and Gy^{-2}, respectively.

Since large single doses are damaging to the normal tissue, radiotherapy is administered in multiple fractions.

By letting d be the dose per fraction, the fractionated dose can be written

$$S_i = e^{-\alpha d} e^{-\beta d^2}. \tag{19}$$

By letting n be the number of fractions,

$$S = \underbrace{e^{-\alpha d}e^{-\beta d^2}...e^{-\alpha d}e^{-\beta d^2}}_{\text{n times}}. \tag{20}$$

Since $D = nd$, Eq. (20) becomes

$$S = e^{-\alpha D\left(1+\frac{d\beta}{\alpha}\right)}. \tag{21}$$

Surviving fraction example: A surviving fraction with value $S = 1$ means that all cells survived the treatment, and $S = 0.3$ means that 3 in 10 cells survived treatment.

While constants α and β can take different values, we use the following estimation $\frac{\alpha}{\beta} \approx 10$.

References

[1] Araujo, R. P., & McElwain, L. S. (2004). A History of the Study of Solid Tumour Growth: The Contribution of Mathematical Modelling. *Bulletin of Mathematical Biology, 66*, 1039-1091.

[2] Bishop, C. M. (2009). Pattern recognition and Machine Learning. Springer, Cambridge.

[3] Burnham, K. P., & Anderson, D. R. (1998). Model selection and inference: a practical information-theoretic approach. Springer-Verlag, New York.

[4] Cancer statistics, 2017. (2017, May 17). Retrieved from http://onlinelibrary.wiley.com/doi/10.3322/caac.21387/full

[5] Chvestov, A. V., Palta, J. J., & Nagata, Y. (2008). Time-dependent cell disintegration kinetics in lung tunors after irradiation. *Physics in Medicine & Biology, 53*, 2413-2423.

[6] Chvetsov, A. V., Dong., L., Palta, J. R., & Amdur, R. J. (2009). Tumor-volume simulation during radiotherapy for head-and-neck cancer using a four-level cell population model. *Int. J. of Radiation Oncology, Biol. Phys., 75* 595–602.

[7] Chvetsov, A. V., Yartsev, S., Schwartz, J. L., & Mayr, N. (2014). Assessment of interpatient heterogeneity in tumor radiosensitivity for nonsmall cell lung cancer using tumor volume variation data. *Medical Physics, 41*(6), 064101

[8] Common Cancer Types. (2017, May 17). Retrieved from https://www.cancer.gov/types/common-cancers

[9] Enderling, H., & Chaplain, M. (2013). Mathematical Modeling of Tumour Growth and Treatment. *Current pharmaceutical design, November*, 1-24.

[10] Frieboes, H. B., Zheng, X., Sun, C. H., Tromberg, B., Gatenby, R. & Cristini, V. (2006). An Integrated Computational/Experimental Model of Tumor Invasion. *Cancer Res 66*, 1597.

[11] Hall, E. J., & Giaccia, A. J. (2012). *Radiobiology for the Radiologist*, (7^{th} ed.) Philadelphia, PA: Lippincott Williams & Willkins.

[12] Hurvich, C. M., & Tsai, C-L. (1989). *Biometrika. 76*(2), 297-307.

[13] Jager, T. (2016). Differential Equations and Likelihood Functions, a refresher. DEBtox Research, De Bilt.

[14] Jain, P., Baker, A., Distefano, G., Scott, A. J., Webster, G. J., & Hatton, M. Q. (2013). Stereotactic ablative radiotherapy in the UK: current status and developments. *BR J Radiol, 86*, 1029.

[15] Jeong, J., Oh, J. H., Sonke, J-J, Belderbos, J. S. A., Bradley, J. D., Fontanella, A. N., Rao, S. S., & Deasy, J. (2017). Modeling the Cellular Response of Lung Cancer to Radiation Therapy for a Broad Range of Fractionation Schedules. *Clinical Cancer Research.*

[16] Metcalfe, P., Kron, T., & Hoban, P. (2002). *The Physics of Radiotherapy X-Rays from Linear Accelerators.* Madison, WI: Medical Physics Publishing.

[17] Non-small Cell Lung Cancer vs. Small Cell: Types, Stages, Symptoms, and Treatment. (2017, August 1). Retrieved from http://www.healthline.com/health/lung-cancer/non-small-cell-lung-cancer-vs-small-cell#1

[18] Risks factors. (2017, May 17). Retrieved from canceratlas.cancer.org/risk-factors/

[19] Sharouni, E. I., Kal, H. B., & Battermann, J. J. (2003). Accelerated regrowth of non-small-cell lung tumours after induction chemotherapy. *British Journal of Cancer, 89* 2184–2189

[20] Tariq, I., Humbert-Vidan, L., Chen, T., South, C., Ezhil, V., Kirkby, N., Jena R, & Nisbet, A. (2014). Mathematical modeling of tumour volume dynamics in response to stereostatic ablative radiotherapy for non-small cell lung cancer. *Physics in Medicine & Biology, 60*, 3695-3713.

[21] Tariq, I. (2016). Adaptive modelling of tumour volume dynamics under radiotherapy (Submitted for the Degree of Doctor of Philosophy). Department of Chemical and Process Engineering, University of Surrey, Guilford.

[22] Tsoularis, A., Wallace, R. (2002). Analysis of logistic growth models. *Mathematical Biosciences, 179*, 21-55.

[23] Types of non-small cell lung cancer. (2017, May 17). Retrieved from https://www.cancer.org/cancer/non-small-cell-lung-cancer/about/what-is-non-small-cell-lung-cancer.html